Journal of Statistical Physics, Vol. 65, Nos. 1/2, 1991

Repeller Structure in a Hierarchical Model. II. Metric Properties

R. Livi,[1,4] A. Politi,[2,4] and S. Ruffo[3,4]

Received March 25, 1991

We study the renormalization dynamics deriving from a hierarchical tight-binding Schrödinger equation. In the Part I of this work we analyzed the topological structure of the recurrent set—a chaotic repeller—and its relation with the spectral problem. In this part we turn our attention to the metric properties of the repeller. We first study periodic orbits and their bifurcation unfolding, and we organize them on a binary tree. We then apply a thermodynamic formalism which provides a complete characterization of the scaling properties of the energy spectrum. The distribution $f(\alpha)$ of local dimensions is determined by computing both a generalized ζ-function through the periodic orbits and the bandwidths of periodic approximants of the Schrödinger operator. When the growth rate R of the potential is smaller than 1, we find evidence of a phase transition, implying that two different classes of states coexist in the spectrum. The asymptotic behavior of the Lebesgue measure μ of the spectrum is also studied. A linear scaling of μ to 0 is observed for $R \to 1_-$, while for $R > 1$, the measure of the periodic approximants goes to 0 as R^{-h} with the hierarchical order h. Finally, we show that the localized state, present for $R < 1$, is characterized by a superexponential scaling of the bandwidth.

KEY WORDS: Hierarchical structures; multifractality; phase transitions; strange repellers; localization.

1. INTRODUCTION

Exactly renormalizable tight-binding Schrödinger operators have been introduced by various authors. Fibonacci potentials[1,2] have been rigorously shown to yield a Cantor-set spectrum.[3-5] An analogous situation is present in hierarchical models as well.[6-8] At variance with the

[1] Dipartimento di Fisica, Università di Firenze, I-50125 Florence, Italy.
[2] Istituto Nazionale di Ottica, I-50125 Florence, Italy.
[3] Dipartimento di Chimica, Università della Basilicata, Potenza, Italy.
[4] Istituto Nazionale di Fisica Nucleare, Sezione di Firenze, Florence, Italy.

0022-4715/91/1000-0073$06.50/0

Fibonacci case, the spectrum presents a transition from absolute to singular continuous at the value $R=1$ of the growth rate of the potential. In Part I of this work[9] we were able to locate and characterize all the components of the spectrum for different values of the parameters. We also discussed the presence of a pure point component located at the upper bound of the spectrum and the associated wavefunctions.

In this paper we turn our attention to the scaling properties of the invariant measure. These properties are related to the scaling indices of physical quantities like the density of states, which have been preliminarly studied also in refs. 6 and 7.

The paper is organized as follows. In Section 2 we briefly recall the main features of the model. In Section 3 we study the bifurcations of periodic orbits of the renormalization transformation as a function of the parameter R. The introduction of a suitable symbolic dynamics allows to show that, for $R>1$, the periodic orbits can be arranged on a complete binary tree. The ordering of trajectories in the symbol plane allows us to develop a simple numerical procedure to compute unstable periodic orbits. In Section 4 we present a detailed multifractal analysis of the repeller and of the energy spectrum, both for $R>1$ and $R<1$. In the latter case, the application of the ζ-function formalism shows in an accurate way the existence of a phase transition in the sense of thermodynamic formalism applied to strange sets. Scaling properties of the asymptotic measure of the energy spectrum are also studied as a by-product of the multifractal analysis. Finally, an anomalous (superexponential) scaling is detected around the largest value of the energy spectrum. Section 5 is devoted to conclusions.

2. THE MODEL

Let us introduce the following discrete one-dimensional Schrödinger operator H[8]:

$$(H\psi)(i) = -[\psi(i+1) - 2\psi(i) + \psi(i-1)] + V(i)\,\psi(i) \tag{2.1}$$

where

$$V(i) = \lambda f(\mathrm{ord}(i)) \tag{2.2}$$

Here i labels the lattice sites, λ is a real parameter giving the strength of the potential, $\mathrm{ord}(i)$ is the largest nonnegative integer j such that 2^j is a divisor of i, and f is a real-valued function defined as follows:

$$f(j) = \frac{R^j - 1}{R - 1} \tag{2.3}$$

where R is chosen to be a positive real parameter. The potential has a peculiar definition in $i=0$:

$$V(0)=\lambda \lim_{j\to\infty} f(j)=\begin{cases}\lambda/(1-R), & R<1\\ \infty, & R\geqslant 1\end{cases}$$

deriving from the equivalence of the semi-infinite with the doubly infinite problem. The eigenvalue problem

$$H\psi(i)=E\psi(i)$$

can be solved by renormalization group.[6–8] This procedure leads to the following recursion equations:

$$\begin{cases}x_{n+1}=2-x_n^2+x_n y_n\\ y_{n+1}=-Rx_n y_n\end{cases} \tag{2.4}$$

with initial conditions $x_0=E-2$ and $y_0=\lambda$, where x_{n+1} and y_{n+1} represent the renormalized energy and potential strength, respectively.

3. PERIODIC ORBITS

The fixed points of Eq. (2.4) in the (x, y) plane are

$$\begin{cases}F1=(-2, 0)\\ F2=(1, 0)\\ F3=(-1/R, (2R^2+R-1)/R)\end{cases}$$

Stability analysis shows that $F1$ and $F2$ have an unstable manifold along the x axis and a stable (unstable) manifold transverse to the x axis for $R<1/2$ ($R>1/2$) and $R<1$ ($R>1$), respectively. The fixed point $F3$ is an unstable focus up to $R=1/2$, where it coincides with the fixed point $F1$, then becoming a saddle for $R>1/2$.

Let us observe that the dynamics of map (2.4) along the x axis coincides with that of logistic map $x'=2-x^2$ at the Ulam point. Accordingly, the interval $[-2, 2]$ is mapped onto itself and the generating partition is made of the two subsegments $[-2, 0)$ and $(0, 2]$ which can be associated wih the symbols 0 and 1, respectively. As a result, each trajectory is converted into a sequence of symbols $(ss)\, s_n$ according to the sign of x_n. It is well known that there is a one-to-one correspondence between infinite ss and initial conditions in the invariant interval. In other words, all sequences are allowed, and, in particular, all periodic sequences exist.

Besides the trajectories belonging to the interval $[-2, 2]$ of the x axis, a fixed point $F3$ and a period-2 orbit have been identified in refs. 7 and 10 which generically lie out of it. In the following we show that such two orbits are nothing but a particular case of an infinite family of trajectories lying out of the x axis, and representing the skeleton of a nontrivial strange repeller. They arise from the familiar periodic orbits of the logistic map through two kinds of bifurcation phenomena that can be investigated by means of a simple linear stability analysis. The linearization of map (2.4),

$$\begin{aligned} \delta x_{n+1} &= (y_n - 2x_n)\,\delta x_n + x_n\,\delta y_n \\ \delta y_{n+1} &= -Ry_n\,\delta x_n - Rx_n\,\delta y_n \end{aligned} \tag{3.1}$$

indicates that the tangent map for all orbits characterized by $y_n = 0$ is of the special type

$$M_n = x_n \begin{pmatrix} -2 & 1 \\ 0 & -R \end{pmatrix} \equiv x_n A_n \tag{3.2}$$

so that x_n plays the role of a multiplicative factor only. Since the eigenvalues of the matrix A_n are equal to -2 and $-R$, the eigenvalues of a periodic orbit are given by

$$m_1 = (-2)^n \prod_{i=1}^{n} x_i, \qquad m_2 = (-R)^n \prod_{i=1}^{n} x_i \tag{3.3}$$

The multiplier m_1 coincides with the eigenvalue of the logistic map at crisis, which is equal to $\pm 2^n$ for all periodic orbits of period n, except for the fixed point $F1$, for which it is equal to 4. Accordingly, the second multiplier turns out to be equal to $\pm R^n$, indicating that all periodic orbits bifurcate at $R = 1$ (except, again, for the fixed point $F1$, which bifurcates at $R = 1/2$). The existence of an infinite family of bifurcations suggests that an infinity of periodic orbits is to be expected out of the x axis. By recalling that the nature of a bifurcation depends on the way the unit circle is crossed by the eigenvalue m_2 of the periodic orbit, here we expect two kinds of bifurcations: (a) period doubling when the sign of the multiplier is negative, (b) double point, i.e., an exchange of stability with another solution, when the sign of the multiplier is positive.[11] From the previous analysis it follows that the information on the sign of the multiplier can be directly retrieved from the parity of the number of 1's occurring in the *ss* associated with the orbit and restricted to one period. Accordingly, we have the following result.

Lemma. All periodic orbits (with $y = 0$) characterized by an odd number of 1's undergo a period-doubling bifurcation ($m_2 = -1$) at $R = 1$.

All periodic orbits (with $y=0$) characterized by an even number of 1's undergo a double-point bifurcation ($m_2=1$) at $R=1$.

In particular, the fixed point $F1$, characterized by a *ss* of 0's, exchanges its stability with the fixed point $F3$, while the fixed point $F2$, characterized by a *ss* of 1's, gives rise to a period-2 solution which exists for $R>1$ only, as already discussed in refs. 7 and 10.

In order to disentangle the structure of the strange repeller, it is now necessary to follow the new branches arising from the above bifurcations. In particular, we perform a numerical analysis of orbits of short period to answer the following questions: (a) unfolding (direct/inverse) of the period-doubling bifurcations; (b) existence of further bifurcations.

We begin with the orbits of period 3, to arrive at 9, with the hope of finding clear evidence of some general law. By scanning all sequences of three bits, it is well known that two independent orbits are found, namely (100) and (110), all the other ones being obtained by rotating the bits, or coinciding with an iterated period-1 trajectory. According to the lemma, the sequence (100) gives rise to a period-6 orbit. The dependence of one of its six values on R is reported in Fig. 1a, from which the direct nature of the period-doubling bifurcation emerges. Still from the lemma, it follows that the sequence (110) is associated with a double-point bifurcation. One of the values assumed by the period-3 solution is reported in Fig. 1b, showing that a new tangent bifurcation occurs at $R=R_c=0.939142....$ In other words, for any R larger than R_c two period-3 solutions exist out of the x axis, emerging from a bifurcation with the trajectory characterized by the *ss* (110). The results of these first numerical simulations can be summarized by stating that: (a) the period-doubling bifurcation is a direct one (as for the fixed point $F2$); and (b) a tangent bifurcation is found at a critical value $R_c<1$.

These two results remain valid after the analysis of all periodic orbits up to period 9, the only difference being the value of R_c. Therefore we propose the following:

Conjecture. An orbit of period n, lying onto the x axis, and containing an odd number of 1's gives rise to one orbit of period $2n$ out of the x axis for $R>1$. An orbit of period n, lying onto the x axis and containing an even number of 1's, gives rise to two orbits of period n out of the x axis for $R>R_c$ ($R_c\leqslant 1$).

Under the hypothesis contained in this conjecture, we can prove a theorem concerning the number of periodic orbits lying out of the x axis for $R>1$.

We denote by $M(n)$ the number of primitive periodic orbits of length

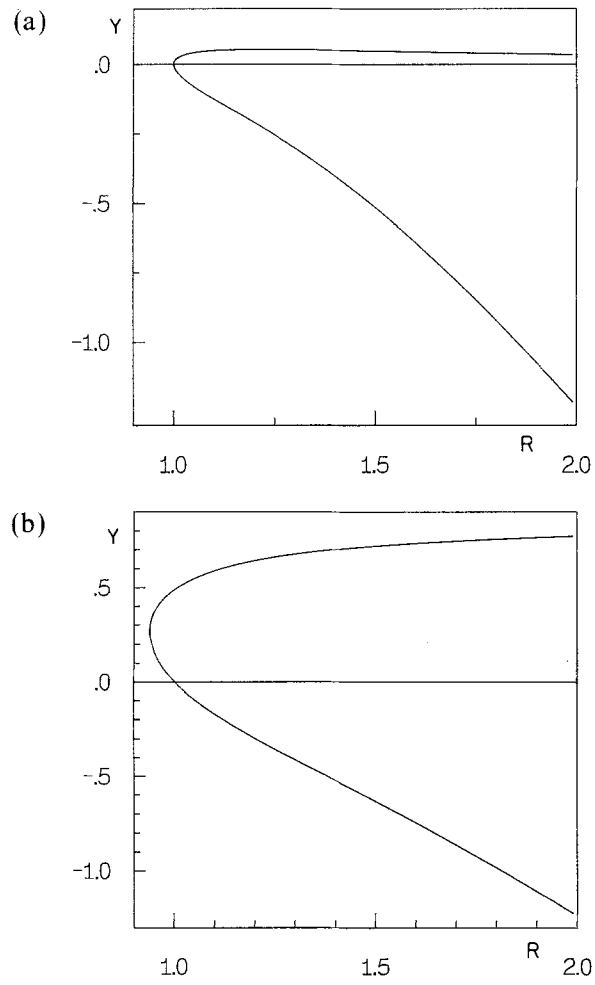

Fig. 1. Bifurcation diagrams of the two period-3 orbits characterized by the symbol sequences (a) 100 and (b) 110. The two branches represent (a) two points of the same orbit of period 6 and *ss UUUDDD*, and (b) two orbits of period 3 and *ss UUD, UDD*.

n of the logistic map, i.e., distinct under rotation of the symbols, and indecomposable in the sum of equal shorter blocks. $M(n)$ can be formally split into two terms: orbits with an even and an odd number of 1's, $M_o(n)$ and $M_e(n)$, respectively.

Theorem. The number of periodic orbits lying out of the x axis for $R > 1$ coincides with the number of orbits with the same period on the x axis, except for one orbit of period 1.

According to the lemma, and from the conjecture, it follows that the theorem can be expressed in terms of the following relations:

$$\begin{aligned} M_o(n) &= M_e(n) && \text{odd } n \\ M_o(n) &= M_e(n) + M_o(n/2) && \text{even } n \end{aligned} \tag{3.4}$$

Before proceeding with the proof, let us also introduce the number $M(n, j)$ of periodic sequences of length n, containing a number j of 1's. Combinatorial analysis allows us to prove that[12]

$$M(n, j) = \frac{1}{n} \sum_{m \mid n, j} \mu(m) \binom{n/m}{j/m} \tag{3.5}$$

where $m \mid n, j$ means that m divides both n and j, and $\mu(m)$ is obtained by inverting the primary relation

$$\sum_{m \mid n} nM(n) = 2^n \tag{3.6}$$

representing the normalization condition (i.e., the total number of *ss* of length n is 2^n). Given the decomposition of a generic m in terms of prime factors $p(m)$ (1 included)

$$m = \prod_{i=1}^{p(m)} q_i \tag{3.7}$$

one has[12]

$$\begin{aligned} \mu(m) &= (-1)^{p(m)} && \text{if } \quad q_i \neq q_j \quad \text{for} \quad \{i \neq j\} \\ \mu(m) &= 0 && \text{otherwise} \end{aligned} \tag{3.8}$$

Equation (3.5) allows us to determine $M_o(n)$,

$$M_o(n) = \frac{1}{n} \sum_{m \mid n} \mu(m) \sum_{m \mid j}^{o} \binom{n/m}{j/n} \tag{3.9}$$

where the "o" in the second sum means that it is restricted to odd j's. A similar expression can be obviously written for $M_e(n)$. We proceed now by considering separately the cases of odd and even n.

(A) If n is odd, then

$$M_o(n) = M_e(n) = \frac{1}{2n} \sum_{m \mid n} \mu(n) 2^{n/m} \tag{3.10}$$

This result follows immediately, by observing that j and $n-j$ have opposite parity, and by a standard relation between binomial coefficients.

(B) If n is even, then

$$M_o(n) = \frac{1}{2n} \sum_{m|n}^{o} \mu(m) 2^{n/m} \tag{3.11}$$

and

$$M_e(n) = M_o(n) + \frac{1}{n} \sum_{m|n}^{e} \mu(m) 2^{n/m} \tag{3.12}$$

where "o" and "e" above the sums indicate that they are restricted to odd and even m's. Indeed, at variance with (A), n/m can be either odd or even, depending on m. In the first case, we are in a condition perfectly equivalent to (A), whereas in the second one, all even submultiples of n contribute to $M_e(n)$ only.

By substituting Eqs. (3.10)–(3.12) into Eq. (3.4), we find that the relation to be proved becomes

$$-\frac{1}{n} \sum_{i|n/2} \mu(2i) 2^{n/2i} = \frac{1}{2n} \sum_{m|n/2}^{o} \mu(m) 2^{n/2m} \tag{3.13}$$

where we have introduced $i = m/2$, as the first sum was restricted to even m's.

To prove Eq. (3.13), we consider separately the cases odd $n/2$ and even $n/2$, as follows:

(B1) From Eqs. (3.7) and (3.8) it is immediately seen that

$$\mu(n) = -\mu(n/2) \tag{3.14}$$

As a result, since $n/2$ odd implies m odd in Eq. (3.13), case B1 is proved.

(B2) If $n/2$ is even, it is sufficient to prove that

$$\sum_{m|n}^{e} \mu(4m) 2^{n/m} = 0 \tag{3.15}$$

where m being even has been redefined as half of its actual value in Eq. (3.13). Again from Eqs. (3.7) and (3.8), we have that

$$\mu(4m) = 0 \tag{3.16}$$

Accordingly, the theorem is proved. QED

As the number of periodic orbits out of the x axis is equal to the number of orbits of the logistic map at crisis, it should be possible to organize them on a full binary tree. Therefore, we should be able to find a generating partition made of two elements only. Since the points (x, y) and $(-x, -y)$ are both mapped onto the same point, any meaningful partition must be able to discriminate between two such points. This is easily guaranteed by splitting the phase space into two regions with a straight line passing through the origin, $y = mx$. The dynamics out of the x axis, for $R > 1$, can be characterized by a sequence of the symbols U (up) and D (down) associated with $y > 0$ and $y < 0$, respectively (that is, $m = 0$). The idea of looking at the sign of y is suggested by the structure of the second equation of map (2.4), which shows that the information on the sign of x (yielding the ss for the logistic map) is directly transferred to the y variable. The sequence of U's and D's of a periodic orbit is determined by the sequence of 0's and 1's of the orbit from which it arises through a bifurcation. Identifying U with 1 and D with 0, the rule is as follows. Given the binary x sequence associated with an orbit of the logistic map, the $(i+1)$st symbol of the y sequence is chosen to be equal to the ith symbol of the y sequence each time the ith symbol of the x sequence is a 0, while it is the negation in the other case. The only ambiguity in the above procedure is, therefore, the starting symbol. However, this is not a problem. Indeed, in the case of an odd number of 1's, a sequence of period $2n$ is generated starting from a sequence of length n, so that the two choices of the initial symbol lead to the same sequence, apart from an irrelevant shift by n units. In the case of an even number of 1's, instead, two distinct sequences are generated corresponding to the two distinct orbits arising from a double-point bifurcation.

3.1. A Method for Computing Periodic Orbits

In order to derive the scaling properties of the recurrent set, one needs an efficient numerical method to compute many unstable periodic orbits and their characteristic exponents. Moreover, the determination of unstable periodic orbits represents the only method to build the skeleton of the chaotic repeller for $R < 1$. In fact, in this parameter range the numerical method developed in ref. 9 is not applicable, as most of the initial conditions are attracted by the interval $x = [-2, 2]$, and, as we will see in the following, there is no way to split the (x, y) plane into two regions containing the repeller and the attractor, respectively.

Let us first consider the case $1/2 < R < 1$. The periodic orbits lying out of the x axis are pairs of unstable foci and saddles arising from a tangent subcritical bifurcation at $R = R_c$. The method to compute these periodic

orbits is based on the existence of invariant manifolds connecting the saddles to the foci and arises from a modification of the method of ref. 9. We start from a point x_0 on the x axis, belonging to a periodic orbit of the logistic map, and such that its *ss* contains an even number of 1's (such orbits are easily found by exploiting the conjugacy of the logistic map with the piecewise linear map $x' = 1 - 2|x|$).[13] Then we choose a point close to x_0 along its stable manifold (i.e., transversely to the x axis) in a given direction, and we start iterating backward according to the inverse of map (2.4). At each step, we always choose the preimage according to the *ss* of x_0. A fast convergence to an unstable focus is observed, provided that we have chosen the right direction and that such an orbit exists (i.e., R is larger than the relative critical value R_c); otherwise, either we observe a divergence to infinity, or the orbit ends up in the noninvertibility region. The consistency of the method proves indirectly that one branch of the stable manifold of x_0 ends on the focus P_F, in analogy with what happens for the focus-saddle pair of fixed points F_1, F_3.

The following step is to consider P_F as the new starting point to reach the conjugated saddle P_S. To this purpose we have to follow the map dynamics along the stable manifold of P_S. In this case, one is faced with the problem of following the stable manifold as closely as possible, in spite of the transverse instability. We proceed as follows: we first compute the two eigenvalues of P_F and we choose two initial conditions P_1 and P_2 close to P_F lying on opposite sides of the less expanding eigenvector. In fact, in analogy with the saddle point x_0, one branch of the stable manifold of P_S ends on the focus P_F and it is tangent to its (less expanding) unstable manifold. Then we need to know whether a given point lies on the left (right) side of the invariant manifold. This can be done by exploiting the ordering of *ss*. In the case of the logistic map (i.e., along the x axis) it is well known that, if $x_2 > x_1$, then $\theta(x_2) > \theta(x_1)$,[14] where the binary expansion of θ is constructed exactly as the Up/Down *ss* discussed in Section 3, with the identification $U \equiv 1$ and $D \equiv 0$. As the stable manifolds of the periodic orbits of the logistic map cannot intersect each other (and so the stable manifolds of the corresponding saddles P_S), the same ordering is maintained out of the x axis. It is therefore sufficient to compare $\theta(P_1)$ $[\theta(P_2)]$ with $\theta(x_0)$ to decide whether P_1 (P_2) stays to the left or to the right of the invariant manifold. Practically, the segment joining P_1 with P_2 is shrunk until its length becomes smaller than a preassigned accuracy. Then, its extrema are iterated according to (2.4) for a given number of time steps and the refinement procedure is again applied to decrease the width. This allows us to move along the stable manifold of P_S until the saddle is finally approached, and a standard Newton method is applied for an accurate estimation of P_S. The periodic orbits for $R = 0.9$ are reported in

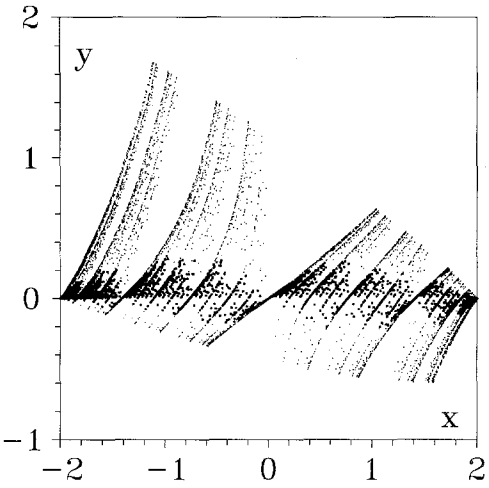

Fig. 2. Periodic orbits of the repeller for $R = 0.9$ (up to period 15). Thick dots denote unstable foci, thin dots refer to the saddles.

Fig. 2, up to period 15. The thick dots indicate the fully unstable component of the repeller lying closer to the x axis.

For $R > 1$ the x axis is fully unstable and all periodic orbits out of it are saddles. Therefore their search is a simpler task. One has to start from any given focus P_F, which now lies on the x axis, and apply the second part of the above procedure, following the stable manifold of the associated periodic orbit out of the x axis. Of course, one must take into account that

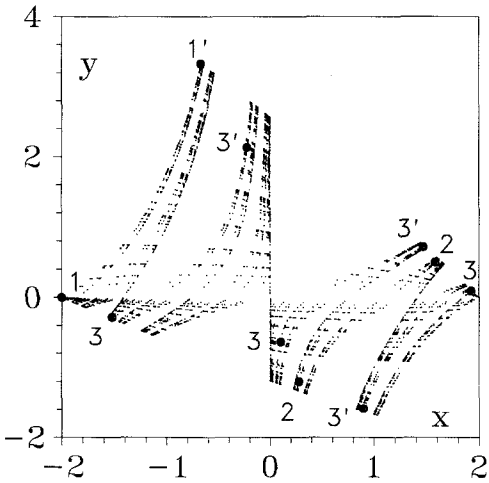

Fig. 3. Periodic orbits of the repeller for $R = 1.5$ (up to period 15). Orbits of period 1, 2, and 3 are explicitly indicated with an obvious meaning of the symbols.

orbits with an odd number of 1's give rise to orbits with a period twice as long, whereas those characterized by an even number of 1's yield two orbits with the same period and lying in opposite directions with respect to the initial orbit. The periodic orbits up to period 15, for $R = 1.5$, are reported in Fig. 3, where the short cycles are explicitly indicated.

4. MULTIFRACTAL PROPERTIES

In this section we study the singularities of the spectrum of the Schrödinger operator (2.1) via the analysis of both the periodic approximants and the periodic orbits of map (2.4) and we compare the results obtained by these two methods.

In the first approach the periodic approximant is defined by truncating the potential at a given hierarchical order h and repeating periodically the structure of the first 2^h sites. In this approximation the spectrum is made of 2^h bands, each one containing the same fraction of states. The basic relation[15] to obtain the multifractal properties of the limit set ($h \to \infty$) is in this case

$$\Gamma(q; h) = \sum_{i=1}^{2^h} \delta_i^{-\tau(q)} \sim 2^{hq} \tag{4.1}$$

where δ_i is the width of the ith band of the periodic approximant and $\tau(q) \equiv (q-1) D(q)$, $D(q)$ being the generalized dimensions. The Legendre transform

$$\alpha = \frac{d\tau(q)}{dq}, \qquad f(\alpha) = \alpha q - \tau(q) \tag{4.2}$$

provides more direct information on the scaling properties. In fact, $f(\alpha)$ coincides with the fractal dimension of the spectral component with scaling index α.

The starting point of the second approach is the definition of the generalized ζ function,[16]

$$\zeta^{-1}(z, \tau) = \prod_p (1 - z^{n_p} m_p^{\tau}) \tag{4.3}$$

where the index p runs over all the primitive periodic orbits and n_p, m_p are their periods and expanding multipliers, respectively. In our case we have to consider the periodic orbits of the renormalization map (2.4). Let us recall that the first zero, z_0, in z of $\zeta^{-1}(z, q)$ is related to the fractal properties of the spectrum through the relation

$$z_0 = e^{-K_0 q} \tag{4.4}$$

where K_0 is the topological entropy and q and τ are defined as in the first approach. The infinite product in Eq. (4.3) can be rewritten as a power series in the z variable; for numerical applications it is truncated at a finite degree k in z and this can be done consistently if all periodic orbits up to period k are known.

It is not obvious that the $\tau(q)$ obtained from Eqs. (4.3) and (4.4) coincides with the one derived directly from Eq. (4.1). In fact, the first method is basically equivalent to studying the intersections of the line of initial conditions ($y=\lambda$) with the stable manifold of the repeller, while in the second case, one takes into account the recurrent set only. Indeed, we will see that the results of the two approaches are essentially coherent apart from some information which cannot be extracted with the second method.

4.1. The Case $R>1$

The application of the first method needs an accurate computation of the bandwidths up to a sufficiently high hierarchical order h. One can show that this can be done by computing the zeros of appropriate polynomials of degree 2^h in E (for more details see refs. 7 and 8). We have observed that all the bands scale exponentially to zero with h, apart from the highest energy band exhibiting a faster scaling. Therefore, it is convenient to analyze only the scaling properties of the first half of the spectrum, discussing separately the contribution originating from the highest band. In fact, it is very reasonable to assume that the remaining part of the spectrum shows asymptotically the same scaling behavior as that of the first half (actually, this has been verified by numerical simulations).

A numerical estimate of $q(\tau)$ is obtained in two steps. First, we compute q_h by means of Eq. (4.1), by comparing two consecutive hierarchical orders,

$$\frac{\Gamma(q;h+1)}{\Gamma(q;h)}=2^{q_h} \tag{4.5}$$

Afterward, we extrapolate the asymptotic value $q(\tau)$ from the sequence of q_h values, having observed an exponential convergence of $(q_{h+1}-q_h)$ with h. The numerical results for $R=1.5$ with a maximum hierarchical order $h=15$ are reported in Fig. 4, displaying the associated $f(\alpha)$ curve. The errors are much smaller than the thickness of the line. Moreover, notice that the minimum and maximum scaling indices $\alpha_{\min}$ and $\alpha_{\max}$ are given by

$$\alpha_{\min}=\frac{\log 2}{\lambda_1}, \qquad \alpha_{\max}=\frac{\log 2}{\lambda_2} \tag{4.6}$$

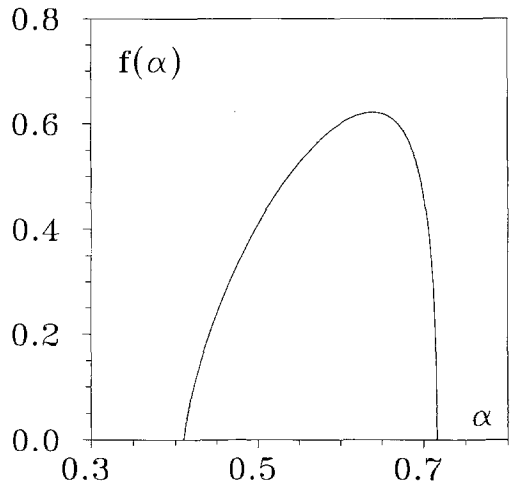

Fig. 4. $f(\alpha)$ curve for $R = 1.5$ as obtained by comparing the bands of hierarchical orders $h = 14$ and 15.

where λ_1 and λ_2 are the Liapunov exponents of the fixed point $F3$ and of the period-4 orbit characterized by the *ss UDDD*, respectively.

An alternative estimate of the $f(\alpha)$ curve has been obtained through the computation of the $\zeta(z)$ function. In this case we have determined the multipliers of all periodic orbits up to period 15. The results are in full agreement with those obtained by the first method. This suggests that the anomalous scaling observed around the highest-energy band can be found only by the first method, which reaveals some singular behavior of the stable manifold.

As a by-product of the multifractal formalism it is also possible to estimate the scaling properties of the Lebesgue measure μ of the energy spectrum. One knows[8] that $\mu = 0$ for $R \geqslant 1$, while it is positive for $R < 1$. The measure of the order-h approximant is defined as

$$\mu(h) \equiv \sum_{i=1}^{2^h} \delta_i \tag{4.7}$$

from which we see that it coincides with Eq. (4.1), specialized to $\tau = -1$. Therefore,

$$\mu(h) \sim 2^{q(-1)h} \tag{4.8}$$

Incidentally, we notice that $q(-1)$ log 2 is nothing but the mean escape time from the repeller.[17] We have computed the Lebesgue measure for

different hierarchical orders h, summing over all the contributions of the bands, including the second half of the spectrum. From the data reported in Table I, one can observe the good agreement between the ratio $\mu(h+1)/\mu(h)$ and $1/R$. This implies that

$$q(-1) = -\frac{\ln R}{\ln 2}, \qquad D(q(-1)) = \frac{\ln 2}{\ln 2R} \tag{4.9}$$

Accordingly, we have an explicit analytic expression at least for one point in the spectrum of the generalized dimensions $D(q)$. It would be nice to prove rigorously Eq. (4.9), but we have not been able to find any precise argument.

4.2. The Case $R < 1$

For $R < 1$ many periodic orbits disappear via tangent bifurcations and half of the remaining cycles are unstable foci, so that they do not contribute to the scaling properties of the energy spectrum, as they cannot be approached along any trajectory. In this range of parameter values, each of the two components of the repeller (saddles and foci) is well described by the symbolic dynamics of the logistic map. For $R = 0.9$, we have computed all periodic orbits up to length 24, aiming to determine possible forbidden sequences and, in turn, to estimate the topological entropy of such components. As a result of the numerical analysis, we have not found any forbidden sequence up to length 13, thus suggesting that the topological

Table I. Asymptotic Ratio of the Lebesgue Measure of the Energy Spectrum between Successive Periodic Approximants for $R > 1$[a]

1.1	0.908266	0.909091
1.2	0.833054	0.833333
1.3	0.769205	0.769231
1.4	0.714281	0.714286
1.5	0.666666	0.666667
1.6	0.624998	0.625000
1.7	0.588235	0.588235

[a] The values of R are listed in the first column; the second column reports the corresponding extrapolated numerical values; the third column contains the teoretical prediction $1/R$.

entropy is log 2, in striking disagreement with the relatively small number of cycles found. However, such an inconsistency disappears if one looks in Fig. 2 at the structure of the recurrent set, which seems to touch the x axis in many (possibly infinite) points, thus suggesting that the closure of the "external" repeller should include some of the cycles on the x axis. In other words, the binary tree is still complete, but the "external" recurrent set and the invariant interval $[-2, 2]$ have in common not only the point $F1$, as for $R > 1$, but also all the cycles whose *ss* have no corresponding trajectory out of the x axis.

The above considerations suggest that the computation of the ζ function from Eq. (4.3) can be performed by factorizing the product into two terms corresponding to the orbits on and out of the x axis, respectively,

$$\zeta^{-1}(z, \tau) = \prod_{\langle 1 \rangle} (1 - z^{n_p} m_p^{\tau}) \prod_{\langle 2 \rangle} (1 - z^{n_p} m_p^{\tau}) \tag{4.10}$$

We can formally multiply and divide the rhs of Eq. (4.10) by all the remaining contributions coming from the orbits on the x axis which do have a counterpart out of the x axis. Accordingly, we can introduce the analytic expression for the ζ function of the logistic map,[18] and we rewrite Eq. (4.10) as

$$\zeta^{-1}(z, \tau) = \frac{(1 - 4^{\tau} z)(1 - 2^{\tau+1} z)}{(1 - 2^{\tau} z)} \frac{\prod_{\langle 2 \rangle} (1 - z^{n_p} m_p^{\tau})}{\prod_{\langle 2' \rangle} (1 - z^{n_p} 2^{\tau n_p})} \tag{4.11}$$

where $\langle 2' \rangle$ indicates the orbits characterized by the same *ss* as those in $\langle 2 \rangle$, but lying on the x axis. To evaluate the multifractal properties of the energy spectrum, we need to identify the smallest zero of Eq. (4.11). It is well known that the first two factors give rise to the well-known phase transition for $\tau = 1$.[19] This is originated from the existence of a single orbit ($F1$) characterized by a Liapunov exponent different from that of all other periodic orbits. In the present case, the orbits of the external component give rise to a further multiplicative contribution which can be expanded in a Taylor series. In Fig. 5 we report $\tau(q)$ obtained from the three contributions in the numerator in Eq. (4.11). As a result, we discover that the contribution of $F1$ is no longer relevant, while a new phase transition appears from the competition between the contribution of the component on the x axis and the external one. A simple interpretation of this result can be given by looking at the $f(\alpha)$ curve plotted in Fig. 6, where both contributions have been drawn. The δ-like component at $\alpha = 1$ [$f(1) = 1$] is the standard distribution of the logistic map, whereas the dashed bell-shaped curve comes from the nontrivial repeller. The two contributions are connected with a typical tangent construction with a slope $q_c \simeq 1.57$.

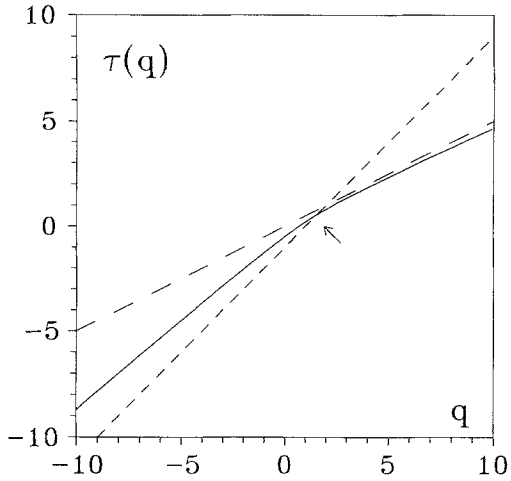

Fig. 5. $\tau(q)$ as resulting from the three smallest zeros of the ζ^{-1} function (4.11) for $R=0.9$. A phase transition occurs at $q_c \simeq 1.57$. Below q_c the leading contribution (smallest τ value) is provided by the orbits with Lyapunov exponent log 2 (dashed curve); above q_c the external component of the repeller dominates (solid curve). The contribution of $F1$ (long-dashed curve) never prevails.

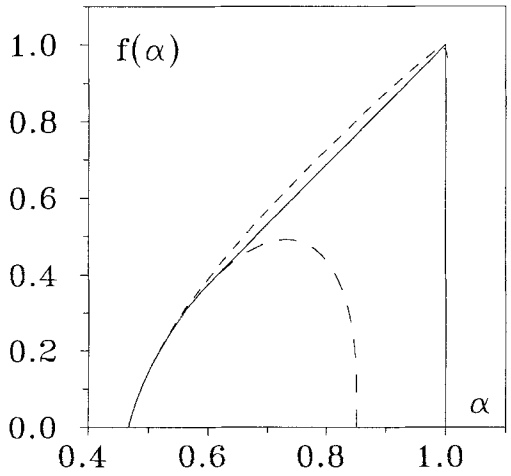

Fig. 6. $f(\alpha)$ curve for $R=0.9$ as obtained from the first pole of the ζ function, after a truncation of the Taylor expansion at the 15th degree (solid curve). The almost linear dashed curve indicates the result of a direct computation from the bandwidths of the periodic approximants of the Schrödinger operator. The dashed bell-shaped curve measures the contribution of the external repeller, which is negligible above $\alpha_c \simeq 0.6$.

Therefore, we can look at the whole recurrent set as the union of two distinct fractal sets (with two different probability weights), each one characterized by its own distribution of scaling indices. Depending on α, one of the components prevails over the other. The transition occurs at $\alpha_c \simeq 0.6$. The smallest scaling index still comes from $F3$ and is given by the expression defined in Eq. (4.6).

Similar results have been also obtained by using the first method described at the beginning of this section, but the convergence to an asymptotic shape is much less clean (see the further dashed curve in Fig. 6). In fact, by this method it is not possible to distinguish between the two components, and, as usual in the case of phase transitions, slowing-down phenomena are at the origin of the poor convergence.

A further relevant point is a possible dependence of the $f(\alpha)$ curve on the choice of the initial value of the potential strength λ in the Schrödinger problem for $1/2 < R < 1$. The possibility to observe a given scaling index α of the density of states around an energy value is related to the existence of an intersection between the line of initial conditions ($y = \lambda$) and the stable manifold of a suitable periodic orbit. Whenever $\lambda < y_m$, where y_m is the smallest y coordinate of the points belonging to a given focus, then the line of initial conditions intersects the stable manifold of a saddle on the x axis, rather than the "external" saddle. As a consequence, one observes the scaling index associated with the saddle on the x axis. Therefore, while decreasing λ, the Liapunov exponents of "external" periodic orbits are progressively substituted by the standard exponents of the logistic map. It is reasonable to expect modifications in the $f(\alpha)$ curve as well. Accordingly, the $f(\alpha)$ curve displayed in Fig. 6 and determined from the periodic orbits has to be interpreted as the distribution for sufficiently large potential strength λ. A numerical verification of this hypothesis is, however, beyond any reasonable computing facility.

For decreasing R, the external component of the repeller keeps decreasing, until it disappears at $R = 1/2$, where $F3$ exchanges the stability with $F1$. Below $R = 1/2$, $F3$ is a focus and does not contribute to the scaling properties of the energy spectrum. Therefore, the $f(\alpha)$ curve reduces of the standard curve of the logistic map.

Let us recall that the measure μ of the spectrum is strictly positive for $R < 1$.[8] Therefore, an interesting question is how it scales to zero for $R \to 1_-$. We have computed the measure for a sequence of periodic approximants and then extrapolated the asymptotic value, having verified an exponential convergence with the hierarchical order, as for the computation of the $f(\alpha)$ curve. The results, shown in Fig. 7, indicate a linear decrease of the asymptotic measure for increasing R toward 1. The prefactor obviously depends on the parameter λ.

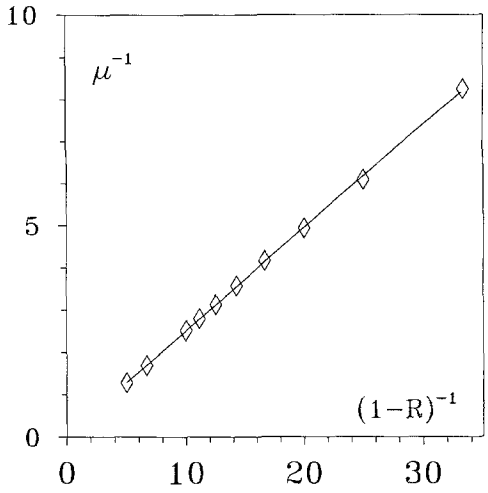

Fig. 7. Inverse of the asymptotic measure μ of the energy spectrum versus $(1-R)^{-1}$. A linear decrease of μ is clearly seen for $R \to 1_-$.

4.3. Anomalous Scaling

In this subsection we explain the mechanism leading to the already mentioned presence of a band showing an anomalous scaling. Let us first recall a result reported in Part I: for $R < 1$, the upper extremum of the spectrum corresponds to the intersection of the line of initial conditions with the unstable manifold of either $F1$ or $F3$ (depending upon whether $R > 1/2$ or $R < 1/2$, respectively). This implies that the scaling properties of the density of states around such a point of the spectrum cannot be inferred from the repeller structure.

The scaling of the width δ of a band sitting around a given energy E of the spectrum can be determined from the dynamical properties of map (2.4). Specifically, an estimate of δ is given by

$$\delta = \frac{1}{m_h} \tag{4.12}$$

where m_h is the largest multiplier computed along the trajectory of length h originating from the point $(E-2, \lambda)$ in the (x, y) plane. In the case of the upper extremum of the spectrum, such an orbit moves along the unstable manifold of $F3$ ($F1$), which asymptotically behaves as (see Part I)

$$y = (1-R)x \tag{4.13}$$

The Jacobian of map (2.4) along such a manifold is [see Eq. (3.1)]

$$M_h = x_h \begin{pmatrix} -(1+R) & 1 \\ -R(1-R) & -R \end{pmatrix} \tag{4.14}$$

Accordingly,

$$m_h = \Lambda^h \prod_i x_i \tag{4.15}$$

where Λ is the largest multiplier of the matrix in Eq. (4.14). From Eqs. (2.4) and (4.13),

$$x_{h+1} \simeq -Rx_h^2 \tag{4.16}$$

from which the leading behavior of x_h is

$$x_h \simeq \exp[2^h] \tag{4.17}$$

By substituting Eq. (4.17) in Eq. (4.15), the leading behavior of m_h is described by

$$m_h \simeq \exp[2^h] \tag{4.18}$$

The superexponential expansion indicated by Eq. (4.18) implies a scaling index around the upper extremum of the spectrum asymptotically equal to 0. This explains the existence of the anomalously narrow band observed numerically. As a consequence, if one considered the whole spectrum, then $f(\alpha)$ would be simply equal to α, for $0 \leqslant \alpha \leqslant 1$.

For $R < 1/2$ the anomalous scaling disappears for $\lambda < |y_3|$, where y_3 is the ordinate of $F3$, as the line of initial conditions intersects the stable manifold of $F1$ (see Part I). In general, let us notice that an anomalous scaling can be detected only around the upper extremum of the spectrum, since $F1$ is the only saddle point on the x axis without a corresponding "external" saddle.

For $R > 1$, the atypical band is displaced to infinite energies. In such a case we can determine the behavior of the multiplier by first estimating the abscissa of the order-h highest band (i.e., the initial condition in the corresponding dynamical problem). From the analysis developed in Part I, the asymptotic slope of the unstable manifold (transverse to the x axis) of $F1$ satisfies the recursive relation

$$\alpha' = \frac{\alpha}{\alpha + R} \tag{4.19}$$

A linear stability analysis indicates that the order of magnitude of the hth iterate of α is, for $R>1$, R^{-h}. Accordingly, the intersection of the line of initial conditions with the corresponding branch of the invariant manifold occurs for $x \simeq R^h$. The multiplier occurring in Eq. (4.12) has now to be computed over h steps starting from (R^h, λ). It is easily seen that the ratio y/x tends asymptotically to $R-1$, as in the previous case, so that we can follow the same procedure. The main difference is the value of the initial condition, which is now already R^h, but it is not sufficient to modify the leading behavior given by Eq. (4.18), which thus remains unchanged for $R>1$.

5. CONCLUSIONS

In this paper we have analyzed the metric properties of the strange repeller associated with map (2.4). We have shown that its unstable periodic orbits characterize the structure of the repeller for any value of R. In particular, observing that map (2.4) reduces on the x axis to the logistic map at the Ulam point, we have been able to describe in full detail the bifurcation mechanisms that locate periodic orbits out of the x axis.

The main results can be summarized as follows. For $0<R<1/2$ the recurrent set reduces to the interval $[-2, 2]$ on the x axis and to the fixed point $F3$. For $1/2<R<1$ a sequence of tangent bifurcations generates pairs of saddles and unstable foci out of the x axis. The saddles and unstable foci belong to two different ergodic components of the recurrent set, A_1 and A_2, respectively. Both components touch together in an infinity of points, corresponding to suitable periodic orbits on the x axis. The fully unstable component A_2 has no practical influence on the scaling properties of the spectrum of the Schrödinger operator. The Lyapunov analysis of the component A_1, combined with the ζ-function formalism, allows us to carry out a detailed multifractal analysis of the spectrum. We find a clear evidence of a phase transition in the $f(\alpha)$ distribution. This is the consequence of the existence of two distinct invariant subsets of A_1: (i) the periodic orbits on the x axis, contributing with the same scaling index, and (ii) the remaining part of the repeller, contributing with a nontrivial distribution. The states associated with the first subset have the same features of the extended states typical of periodic potentials, while those associated with the second subset should reasonably show a sort of self-similar structure as found in the Fibonacci problem.[20] The only aspect which is not captured by this formalism is a superexponential scaling detected at the upper edge of the spectrum, which has been tackled by other means.

At $R=1$ all periodic orbits on the x axis undergo either double-point or period-doubling bifurcations. As a result, the unstable foci become

saddles and other saddles are generated by period-doubling, so that, for $R > 1$ the recurrent set is made of a single component out of the x axis. All the periodic orbits can be organized on a full binary tree. The symbolic dynamics follows from the introduction of a simple generating partition determined by the sign of the variable.

All these results, together with those obtained in Part I, provide a detailed and, hopefully, complete description of the recurrent set (a strange repeller) associated with map (2.4). Let us observe that the analytical and numerical techniques applied to this problem can in principle be applied to similar problems. In fact, it results that a *dynamical* approach is interesting not only for studying nonlinear maps, but it also provides all the main information about the associated spectral problem.

It is worth mentioning that this *dynamical* approach provides further information with respect to resolvent methods.[8] An obvious example concerns the scaling properties of the energy spectrum. A less straightforward result is the possibility of identifying detailed properties of the eigenstates. In our case, the existence of a pure-point component (for $R < 1$) is the direct consequence of the study of the properties of the invariant manifolds.

ACKNOWLEDGMENTS

We acknowledge useful discussions with J. Bellissard, H. Kunz, R. Lima, L. Pastur, M. Rasetti, and A. Sütó.

REFERENCES

1. M. Kohmoto, L. P. Kadanoff, and C. Tang, *Phys. Rev. Lett.* **50**:1870 (1983).
2. S. Ostlund, R. Pandit, D. Rand, H. J. Schellnhuber, and E. D. Siggia, *Phys. Rev. Lett.* **50**:1873 (1983).
3. M. Casdagli, *Commun. Math. Phys.* **107**:292 (1986).
4. A. Sütó, *Commun. Math. Phys.* **111**:409 (1987).
5. A. Sütó, *J. Stat. Phys.*, to appear.
6. T. Schneider, D. Wurtz, A. Politi, and M. Zannetti, *Phys. Rev. B* **36**:1789 (1987).
7. R. Livi, A. Maritan, and S. Ruffo, *J. Stat. Phys.* **52**:595 (1988).
8. H. Kunz, R. Livi, and A. Sütó, *Commun. Math. Phys.* **122**:643 (1989).
9. R. Livi, A. Politi, and S. Ruffo, Repeller structure in a hierarchical model. I. Topological properties, *J. Stat. Phys.*, this issue.
10. D. Würtz, T. Schneider, A. Politi, and M. Zannetti, *Phys. Rev. B* **39**:7829 (1989).
11. G. Iooss and D. D. Joseph, *Elementary Stability and Bifurcation Theory* (Springer, New York, 1980).
12. G. H. Hardy and E. M. Wright, *An Introduction to the Theory of Numbers* (Oxford University Press, Oxford, 1979).
13. P. Collet and J. P. Eckmann, *Iterated Maps of the Interval and Dynamical Systems* (Birkhäuser, Boston, 1980).

14. P. Grassberger, *Z. Naturforsch.* **43A**:671 (1988).
15. T. C. Halsey, M. H. Jensen, L. P. Kadanoff, I. Procaccia, and B. I. Shraiman, *Phys. Rev. A* **33**:1141 (1986).
16. P. Cvitanovic, *Phys. Rev. Lett.* **61**:2729 (1988).
17. T. Tél, in *Directions in Chaos*, Vol. 3, *Experimental Study and Characterization of Chaos*, Hao Bai Lin, ed. (World Scientific, Singapore, 1990).
18. R. Artuso, E. Aurell, and P. Cvitanovic, *Nonlinearity* **3**:325 (1990).
19. D. Katzen and I. Procaccia, *Phys. Rev. Lett.* **58**:169 (1987).
20. M. Kohmoto, B. Sutherland, and C. Tang, *Phys. Rev. B* **35**:1020 (1987).